Scientia Iranica C (2018) 25(3), 1395–1411

SCIENTIA IRANICA

Sharif University of Technology
Scientia Iranica
Transactions C: Chemistry and Chemical Engineering
http://scientiairanica.sharif.edu

2,4-dichlorophenoxyacetic acid adsorption from contaminated water through activated carbon reclaimed with zero-valent iron and titanium dioxide

Sh. Jokar Baloochi, A.R. Solaimany Nazar*, M. Farhadian, and A. Goshadrou

Department of Chemical Engineering, Faculty of Engineering, University of Isfahan, Isfahan, Iran.

Received 21 August 2017; received in revised form 25 December 2017; accepted 16 April 2018

KEYWORDS
2,4-dichlorophenoxyacetic acid;
Adsorption;
Activated carbon;
Zero-valent iron;
Titanium dioxide.

Abstract. The sol-gel method was used for the synthesis of zero-valent iron/titanium dioxide supported on activated carbon (Fe^0/TiO_2/AC) adsorbents, and the adsorbents were comprehensively characterized by XRF, XRD, FT-IR, BET, FE-SEM, and EDX analyses. The batch experiments were performed to evaluate the effect of adsorbent type, pH of solution, pollutant initial concentration, and contact time on the 2,4-dichlorophenoxyacetic acid (2,4-D) adsorption efficiency. The equilibrium experiments revealed that the Langmuir isotherm was in good agreement with the adsorption equilibrium data, whereas the adsorption kinetic experiments indicated that the adsorption procedure was described perfectly through a pseudo-first-order kinetic model. The obtained maximum adsorption capacities from Langmuir isotherms of 86.5, 87.5, 86,57, and 88.76 mg/g were achieved for Activated Carbon (AC), zero-valent iron/activated carbon (Fe^0/AC), titanium dioxide/activated carbon (TiO_2/AC), and Fe^0/TiO_2/AC at the 2,4-D initial concentration of 90 mg/L, pH = 4 and 25°C, respectively.

1. Introduction

Improving the quality of agricultural products and pest control has been the main application of pesticide consumption in recent years [1,2]. 2,4-dichlorophenoxyacetic acid (2,4-D) is a current herbicide, due to its high selectivity and economy [3], which controls broad leaf weeds [1,4-8]. The maximum allowable amount of 2,4-D is 0.03 mg/L in an aqueous medium [9]. The main features of 2,4-D include relative toxicity with high movability and durability in an aqueous medium [10]. Other properties of 2,4-D include being non-volatile and highly soluble in water [7]. The half-life of 2,4-D is within 6-170 days in an aqueous medium [11]; thus, removing this herbicide from contaminated water depends on the quantitative and qualitative acceptors of water resource. Contamination of surface water and groundwater by 2,4-D can lead to serious threats, such as cancer and reproductive problem, to human health [6]; therefore, it is necessary to remove this contaminant from water sources.

Adsorption, nanofiltration, electrocoagulation, photocatalytic degradation, photo-fenton, ultrasound, biological processes, and sedimentation are the common methods for treatment of the contaminated water containing pesticides [1,2]. The removal of pesticides by chemical coagulation, photo oxidation, sedimentation, filtration, and adsorption depends on the chemical nature of pesticide and the mechanism of the process [12]. Utilization of different methods, such as

*. *Corresponding author. Tel: +98 31 37934027; Fax: +98 31 37934031*
E-mail addresses: Shahrokh.jokar@gmail.com (Sh. Jokar Baloochi); asolaimany@eng.ui.ac.ir (A.R. Solaimany Nazar); m.farhadian@eng.ui.ac.ir (M. Farhadian); a.goshadrou@eng.ui.ac.ir (A. Goshadrou)

doi: 10.24200/sci.2018.5053.1066

adsorption, nanofiltration, advanced oxidation process, photo-catalytic degradation, photo-Fenton, biological oxidation, and aerobic degradation, has been introduced for 2,4-D elimination [3].

The removal of pesticides from an aquatic environment has been carried out by different adsorbents and photocatalysts. Recently, nanocomposites and bio nanocomposites have been used to remove pesticides [13]. Different adsorbents have been used to remove pesticides in previous studies including rice husk [14,15], Activated Carbon (AC) [16-18], zeolites [19,20], montmorillonite and bentonite [21], and calcite and kaolinite [22]. In addition, biopolymers, such as chitosan [23,24] and alginate [24], have been used for the pesticides adsorption. Porous structure, economy, accessibility, and mechanical strength are the promising features of an AC adsorbent [25]. In recent researches, several adsorbents have been applied to adsorption of 2,4-D that include activated carbon-based data palm pits [1], activated carbon from wood composite [2], adsorbents prepared from groundnut shell (GSA, GSC, and GSAC) [3], single-walled carbon nanotube [4], MIEX resin [5], activated carbon fiber modified by nitric acid [6], Langsat Empty Fruit Bunch Activated Carbon (LEFBAC) [7], pumpkin seed hull activated carbon [10], rice husk ash [15], granular activated carbon [26], modified granular activated carbon [27], activated carbon from date stones (DSAC) [28], Coconut Activated Carbon (CAC) [29], Corncob Activated Carbon (CCAC) [30], Coconut Shell Activated Carbon (CSAC) [31], activated carbon prepared from barhi date seeds (BDSAC) [32], Granular Activated Carbon Filtersorb 300 (GAC-F300) [33], and graphitic carbon nanostructures prepared from biomass [34].

Nanoparticles have a significant degradation performance because of their great surface area and favorable adsorption capacity [35]. The superior reactivity of Zero-Valent Iron (ZVI) nanoparticles is because of the high specific surface area [36]. Because of the high surface energy and natural magnetic interaction, this nanoparticle has a high inclination for cumulation. The aggregation of nanoparticles reduces the surface area, mobility, and activity [37]. As ZVI is exposed to air, it is oxidized which loses its high activity [38]. In order to prevent the aggregation, the nanoparticles are impregnated into a base substance like AC [25,39-41], graphite [42], silica [43,44], bentonite [45], or a membrane [46,47].

Titanium dioxide nanoparticles have high oxidation capability and are non-toxic, cheap and lightly stable [48]. However, their application in a treatment process is limited due to the low adsorption capacity [49]. BET analysis showed that titanium dioxide powder with anatase and rutile phases had specific surface area of about 67 m^2/g [50]. Materials such as biopolymer nanofibers [51], cotton fiber [52], Al_2O_3 [53], SiO_2 [54], and AC [49,55-60] are applied as the support for titanium dioxide nanoparticle. It has been reported that using silica, glass, polystyrene spheres, and AC as supports for TiO_2 led to higher photocatalytic activity and surface area [61].

Applying adsorption as a treatment process will cause secondary pollution that is unfavorable. In contrary, AOP enjoys several advantages: rapid reaction rate, lack of sludge production, and high potential for toxicity reduction. However, AOP is much more complex than the adsorption and needs major investments, which can be counted as disadvantageous. To the best of our knowledge, the performance of $Fe^0/TiO_2/AC$ for 2,4-D adsorption has not been studied in previous studies. The main approach to future researches includes adopting simultaneous adsorption and AOP together. The synergistic effect between adsorption and AOP is an important issue as the impregnation of the AC with nanoparticles may result in pore collapse and lose active sites for adsorption. The present study investigates the effect of AC impregnation with nanoparticles on the adsorption capacity of 2,4-D from an aqueous medium without light illumination.

In this research, the reduction liquid phase method was applied to Fe^0/AC adsorbent synthesis and the sol-gel technique was used for TiO_2/AC, ZVI/TiO_2 based on the AC ($Fe^0/TiO_2/AC$) adsorbents. The adsorbents were specified comprehensively by XRF, XRD, FT-IR, FE-SEM, EDX, and BET analyses. The adsorption process and adsorption capacity of (2,4-D) of the adsorbents were evaluated by kinetics and adsorption equilibrium studies in a series of batch experiments.

2. Materials and methods

2.1. Adsorbate

2,4-D with 97% purity was prepared from Sigma-Aldrich and applied as the adsorbate. The molecular weight and maximum UV absorption of 2,4-D are 221.04 g/mol and 284 nm. In addition, 2,4-D solubility in water is 900 mg/L at 293 K [2]. The standard stock solution was prepared by dissolving a sufficient amount of 2,4-D in distilled water. All other chemicals were of analytical grade and applied without any further purification.

2.2. Adsorbents preparation

The precursors of titanium dioxide and ZVI include titanium tetrachloride ($TiCl_4$) and iron (II) sulfate hydrate ($FeSO_4.7H_2O$), respectively. The sol-gel method was adopted for synthesizing the $Fe^0/TiO_2/AC$ adsorbent. Firstly, a solution consisting of 72 ml of ethanol and 18 ml of deionized water (ethanol/deionized water: 4/1 v/v) was prepared in a three-neck flask, and 7 ml of $TiCl_4$ was mixed with 56 ml of deionized water.

The $TiCl_4$ solution was added slowly into the three-neck flask, 0.25 g of $FeSO_4.7H_2O$ was poured, and then the flask was placed in an ultrasonic water bath for 20 min. Afterwards, the solution was mixed by a magnetic stirrer for 30 min. 50 ml of 1 M solution of sodium borohydride ($NaBH_4$) was gradually added drop-wise to the prepared solution at 5-7 ml/min rate. Likewise, the solution was mixed well using a magnetic stirrer for 30 min. Consequently, 4.95 g of AC was poured gradually into the solution, and the mixture was agitated for 1 h. The final solution was placed at ambient temperature for 24 h. Then, the solution was filtered and washed with ethanol in two stages and placed in an oven at 120°C for 2 h. The calcination process was performed to complete the synthesis process in a furnace at 400°C for 2 h. Finally, the synthesized adsorbent was poured into a black bottle and kept there at 15-20°C until use. The mass ratio of Fe^0 to TiO_2 was 1%. Adsorbents Fe^0/AC and TiO_2/AC were synthesized similarly according to the above-mentioned procedure.

2.3. Characterization of adsorbents

X-Ray Fluorescence (XRF) analysis (Bruker, Model S4 Pioneer, Germany) was performed to specify the adsorbents composition. X-Ray Diffraction (XRD) was accomplished with a XRD diffractometer (Bruker, Model D8 Advance, Germany) within the scanning range of $2\theta = 10° - 80°$. For the analysis of XRD peaks, the X'Pert HighScore software was used. The point of zero charge (pH_{PZC}) of the adsorbents was measured according to the procedure described by Reddy et al. (2010) [62]. Fourier transform infrared (FTIR) spectroscopy analysis was carried out by a FTIR spectrometer (Jasco, Model 6300, Japan) within a scanning range of 400-4000 cm^{-1} to determine the surface functional groups and surface chemical characteristics of the adsorbents. The surface physical properties were identified by a Brunauer-Emmett-Teller (BET) (Microtrac Bel Corp, Model Belsorp mini, Japan) analysis. The Nitrogen adsorption was used to specify surface area and porosity attributes at 77 K. The surface morphology of adsorbents and their particle size distributions were characterized by Field Emission Scanning Electron Microscopy (FE-SEM) (Zeiss, Model Sigma-VP 500, Germany) analysis. Elemental analysis was performed using Energy Dispersive X-ray (EDX) (Oxford Instrument, England).

2.4. Batch adsorption studies

The batch equilibrium experiments were accomplished in 50-ml Erlenmeyer flasks containing 0.02 g of adsorbent and 20 ml of 2,4-D solution with different initial concentrations (15-90 mg/L) and pHs (4, 7, and 10). The flasks were agitated for 6 to 8 h in a shaking incubator (N-Biotek, Model NB-205v, South Korea) at 130 rpm and 25°C. After adsorption contact, the sample was centrifuged (Hanil, Model supra 22-k, South Korea) at 15000 rpm for 10 min. The 2,4-D concentration was analyzed by an UV-Vis spectrophotometer (Jasco, Model V-570, Japan) at the wavelength of 283 nm. The pH of solution was adjusted through adding 1 M sodium hydroxide and 0.1 M sulfuric acid and measured by a pH meter (Elmetron, Model CP-505, Poland).

The adsorbed 2,4-D capacity at time t, q_t (mg of adsorbate/g of adsorbent) and the removal efficiency of 2,4-D, E(%) were calculated through Eqs. (1) and (2), respectively:

$$q_t = \frac{(C_0 - C_t)V}{m}, \tag{1}$$

$$E\% = \frac{C_0 - C_t}{C_0} \times 100, \tag{2}$$

where C_0 (mg/L) and C_t (mg/L) are the initial concentration and concentration at time t, respectively, V (L) is the solution volume, and m (g) is the adsorbent mass. The adsorption equilibrium capacity, q_e (mg of adsorbate/g of adsorbent), is determined by Eq. (3):

$$q_e = \frac{(C_0 - C_e)V}{m}, \tag{3}$$

where C_e (mg/L) is the 2,4-D equilibrium concentration.

For AC, Fe^0/AC, and TiO_2/AC adsorbents, the equilibrium was achieved after 4 h, while, in the case of Fe^0/TiO_2/AC, it was 6 h. To ensure the equilibrium condition, the adsorption experiments were performed within 6 to 8 h.

3. Results and discussion

3.1. Adsorbents characterization

The results of XRF analysis are shown in Table 1. The results show that the weight percentages of Fe^0, TiO_2, and the total Fe^0 and TiO_2 are almost identical in the Fe^0/AC, TiO_2/AC, and Fe^0/TiO_2/AC adsorbents, respectively. In addition, the weight ratio of Fe^0 to TiO_2 in Fe^0/TiO_2/AC adsorbent is close to 1%.

The XRD patterns of AC, Fe^0/AC, TiO_2/AC, and Fe^0/TiO_2/AC adsorbents are illustrated in Figure 1. The XRD of AC (Figure 1(a)) shows a peak at about 24.4° (002) which corresponds to the reflection of aromatic layers in carbon on the (002) plane. This peak indicates an amorphous structure present in the AC adsorbent. The corresponding peaks occur at 26.4°, 23.47°, and 23.45° for Fe^0/AC (Figure 1(b)), TiO_2/AC (Figure 1(c)), and Fe^0/TiO_2/AC (Figure 1(d)), respectively.

An obvious peak of Fe^0 is observed at 44.7°(110) and 44.05° in Fe^0/AC and Fe^0/TiO_2/AC adsorbents,

Table 1. XRF analysis of Fe^0/AC, TiO_2/AC, and Fe^0/TiO_2/AC nanocomposites (weight%).

Compound	Fe^0/AC	TiO_2/AC	Fe^0/TiO_2/AC
TiO_2	–	14.75	15.11
Fe_2O_3	20.83	0.03	0.258
SO_3	4.82	0.076	0.164
Na_2O	3.72	–	0.14
Al_2O_3	0.27	1.34	1.37
SiO_2	0.17	0.204	0.13
P_2O_5	0.14	0.138	0.096
CaO	0.12	0.22	0.103
Cl	0.034	3.06	1.91
K_2O	0.025	0.107	0.028
MnO	0.024	–	–
CuO	0.011	0.004	–
ZnO	0.005	–	–
LOI	69.75	80.03	80.62
Total	99.92	99.96	99.93

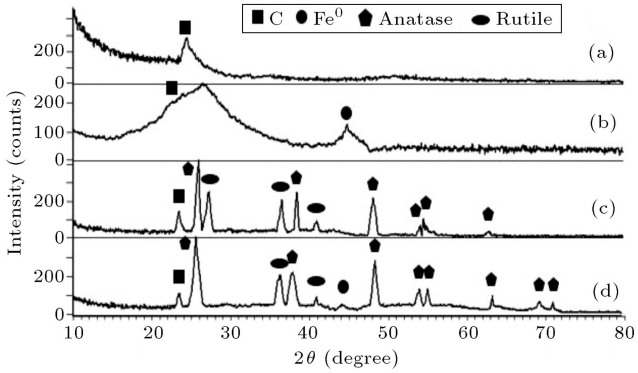

Figure 1. XRD Patterns of (a) AC, (b) Fe^0/AC, (c) TiO_2/AC, and (d) Fe^0/TiO_2/AC.

respectively, indicating the low oxidation level. The peak of Fe^0 shows good crystallinity of Fe^0.

The six diffraction peaks of anatase TiO_2 are observed clearly at 25.9° (101), 38.4° (004), 48.1° (200), 54.1° (105), 54.8° (211), and 62.8° (204) for TiO_2/AC. In addition, for TiO_2/AC adsorbent, the rutile peaks of TiO_2 occur at 27.25° (110), 36.5° (101), 40.97° (111), and 54.3° (211).

Similarly, the peaks of anatase TiO_2 for Fe^0/TiO_2/AC are observed at 25.6°, 37.9°, 48.36°, 53.96°, 55.03°, 63.2°, 69.2°, and 70.8°. The two peaks of rutile TiO_2 are observed at 36.3° and 40.92°. The XRD patterns of TiO_2/AC and Fe^0/TiO_2/AC reveal the formation of mixed phases in the adsorbents.

The FT-IR spectroscopy explains the presence of functional groups on the adsorbents surface. The FT-IR spectra of AC, Fe^0/AC, TiO_2/AC, and Fe^0/TiO_2/AC are shown in Figure 2. The FT-IR spectrum of AC (Figure 2(a)) has a broad peak at 3436.5 cm^{-1}, which is attributed to the –OH stretch vibration of a hydroxyl group. The absorbance peak at 1703.8 cm^{-1} shows the C=O stretching vibration of carbonyl and carboxyl groups. The band at 1564 cm^{-1} is related to the C=C stretching of the aromatic group. The peak at 1430.9 cm^{-1} corresponds to the –C-H bending vibration of the alkane group. The absorbance peaks at 1117.6 and 1066.4 cm^{-1} describe the C-O stretch vibrations and show the presence of the hydroxyl, ether and ester functional groups. The bands at 799.3 and 876.5 cm^{-1} are relevant to the C-Cl stretching vibration of alkyl halide. The final peak at 610.4 cm^{-1} is attributed to the C-Cl stretching vibration of alkyl halide. In the FT-IR spectrum of Fe^0/AC (Figure 2(b)), five different peaks' intensities exist at 465.7 cm^{-1}, 615.2 cm^{-1}, 1112.7 cm^{-1}, 1565 cm^{-1}, and 3423 cm^{-1} that illustrate the hematite (α-Fe_2O_3) [63], maghemite (γ-Fe_2O_3) [63], γ-FeOOH-lepidocrocite [63], C=C stretch vibration [64], and O-H stretching vibration of hydroxyl group. 1155.2 cm^{-1}, 1571.7 cm^{-1}, 1720.2 cm^{-1}, and 3428 cm^{-1} of FT-IR spectrum of TiO_2/AC (Figure 2(c)) exhibit Ti-O functional group of TiO_2 nanoparticles [65], C=C stretch vibration [64], C=O stretch vibration [64], and O-H stretching vibration of a hydroxyl group. In the spectrum of Fe^0/TiO_2/AC nanocomposite (Figure 2(d)), five different peaks' intensities are observed at 669.2 cm^{-1}, 1136.8 cm^{-1}, 1576.5 cm^{-1}, 1720.2 cm^{-1}, and 3391.2 cm^{-1} that indicate the symmetric Fe-O stretch [63], Ti-O functional group of TiO_2 nanoparticles [65], C=C stretch vibration [64], C=O stretch vibration [64], and O-H stretching vibration of H_2O [63], respectively.

The BET surface area, Langmuir surface area, total pore volume, and average pore diameter are achieved through the nitrogen adsorption-desorption. Figure 3 indicates the nitrogen adsorption and desorption for AC (Figure 3(a)), Fe^0/AC (Figure 3(b)), TiO_2/AC (Figure 3(c)), and Fe^0/TiO_2/AC (Figure 3(d)) at 77 K. The obtained isotherms have a typical type IV with a H3 hysteresis loop. The isotherms of AC, Fe^0/AC, TiO_2/AC, and Fe^0/TiO_2/AC adsorbents indicate a remarkable improvement of relative pressure at the P/P_0 less than 0.1 to about 0.2, exhibiting that all adsorbents are microporous. In addition, the mesoporous structures' presence is identified with respect to the closure of hysteresis loops at relative pressure rates of $P/P_0 = 0.3026$ (AC), $P/P_0 = 0.2982$ (Fe^0/AC), $P/P_0 = 0.3003$ (TiO_2/AC), and $P/P_0 = 0.3998$ (Fe^0/TiO_2/AC).

Table 2 indicates the surface and pore properties of the adsorbents. The specific surface areas of Fe^0/AC, TiO_2/AC, and Fe^0/TiO_2/AC adsorbents decrease compared to that for the AC, which may be due to the occupation of the AC surface with Fe^0 and TiO_2 nanoparticles. Accordingly, the porosity decreases due

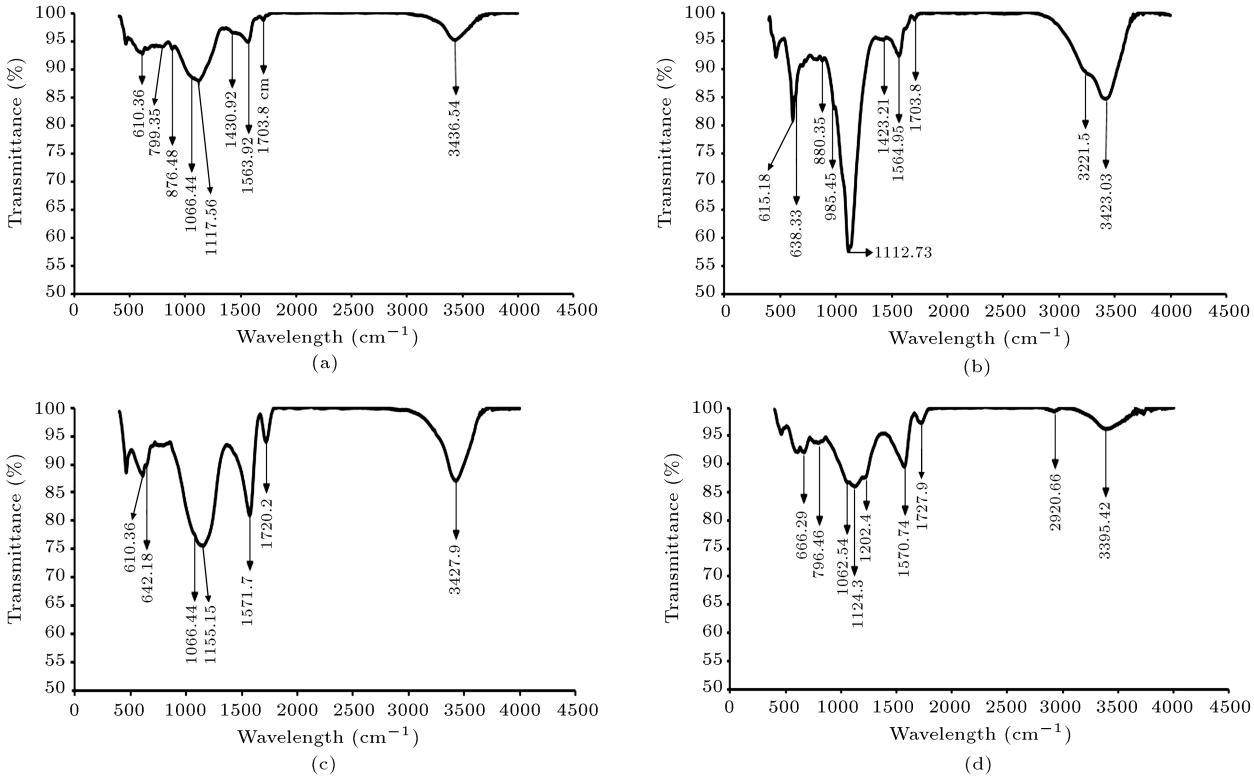

Figure 2. FT-IR spectra of: (a) AC, (b) Fe^0/AC, (c) TiO_2/AC, and (d) Fe^0/TiO_2/AC.

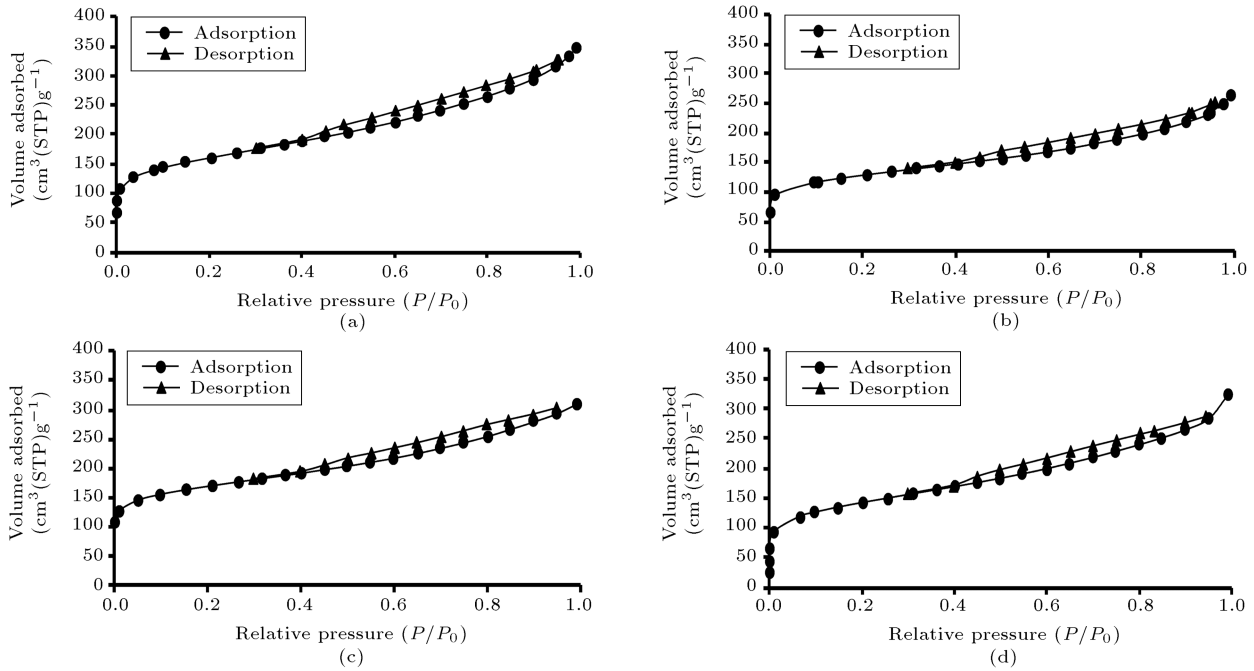

Figure 3. Nitrogen adsorption-desorption isotherms and surface characteristics of: (a) AC, (b) Fe^0/AC, (c) TiO_2/AC, and (d) Fe^0/TiO_2/AC.

to pore collapse caused by the impregnation of AC with nanoparticles.

The morphological structures of AC, Fe^0/AC, TiO_2/AC, and Fe^0/TiO_2/AC adsorbents were analyzed by FE-SEM micrograph. As shown in Figure 4, the AC support indicates a uniform morphology and slit-shaped pores. The surface of Fe^0/AC showed a few agglomerations in some local areas (Figure 4(b)). A comparison of the AC and the synthesized adsorbents' morphological structure indicates the presence of a new

Table 2. Surface characteristic of AC, Fe^0/AC, TiO_2/AC, and Fe^0/TiO_2/AC adsorbents.

Physical parameters	AC	Fe^0/AC	TiO_2/AC	Fe^0/TiO_2/AC
BET surface area (m^2/g)	447.66	364.56	447.16	402.13
Langmuir surface area (m^2/g)	481.38	414.91	569.73	420.51
External surface area (m^2/g)	78.43	49.58	50.83	66.82
Micropore surface area (m^2/g)	369.23	314.98	396.33	335.31
Total pore volume (cm^3/g)	0.53	0.403	0.479	0.496
Micropore volume (cm^3/g)	0.352	0.273	0.368	0.322
Average pore diameter (nm)	4.739	4.422	4.284	4.937

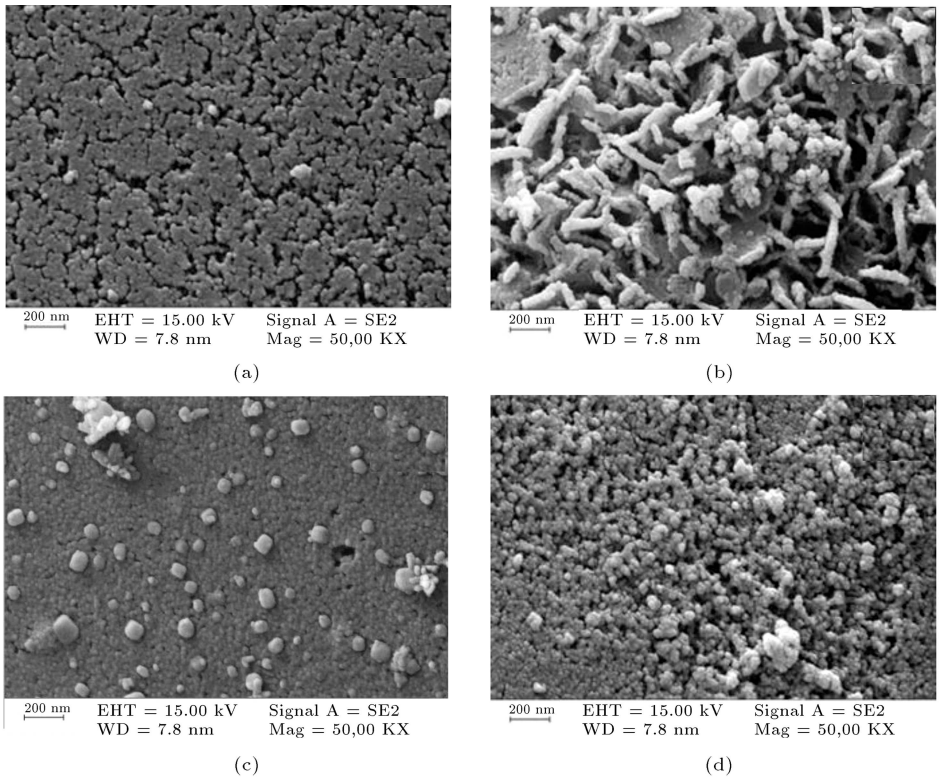

Figure 4. FE-SEM micrograph of: (a) AC, (b) Fe^0/AC, (c) TiO_2/AC, and (d) Fe^0/TiO_2/AC.

structure due to the impregnation process. The FE-SEM micrograph shows mesoporous and microporous surfaces of AC, whereas the nanoparticles are deposited onto the external surface.

The EDX spectrum of adsorbents is shown in Figure 5. The EDX spectrum of AC (Figure 5(a)) indicates that carbon is the main element. Similarly, the EDX spectrum of Fe^0/AC (Figure 5(b)), TiO_2/AC (Figure 5(c)), and Fe^0/TiO_2/AC (Figure 5(d)) adsorbents indicates the presence of C; Fe, C;Ti;O and C; Fe;Ti;O as the main elements, confirming the successful synthesis of the adsorbents.

3.2. Effect of solution pH on the 2,4-D adsorption

In an adsorption process mechanism, adsorption medium pH displays a significant role in a pollution treatment [2]. The electrostatic interactions between adsorbent and adsorbate are controlled with pH [66]. The characteristics, such as the adsorbent surface charge, ionization degree, and speciation of adsorbate, are dependent on pH solution [26]. The 2,4-D dissociation constant is 2.73 at 25°C [4].

The protonated and deprotonated species exist when the solution pH is below 2 and above 4.5, respectively [67]. Therefore, at higher pH, the 2,4-D is separated and their higher ratio exists in the anion form in the water solution. The effect of solution pH on the removal efficiency of 2,4-D and adsorption equilibrium capacity (q_e) of 2,4-D by adsorbents was investigated at 4,7,10 the pH values, with the initial concentration of 90 mg/L at 25°C. The pH_{PZC} is measured 6.6, 6.8, 6.2, and 6.35 for AC, Fe^0/AC, TiO_2/AC, and Fe^0/TiO_2/AC adsorbents, respectively.

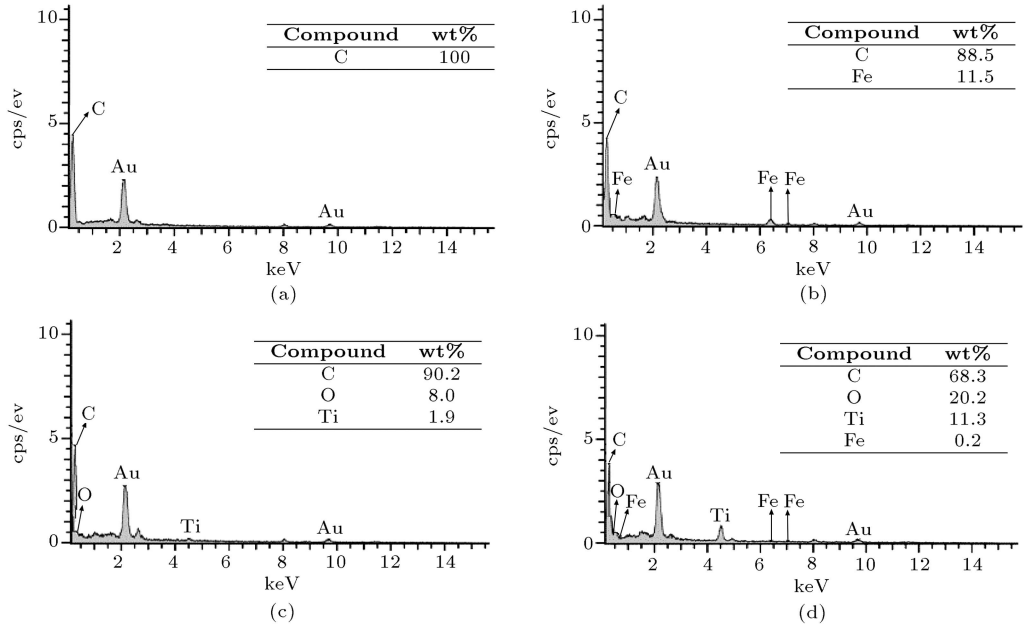

Figure 5. EDX spectrum and XRF analysis of: (a) AC, (b) Fe^0/AC, (c) TiO_2/AC, and (d) Fe^0/TiO_2/AC.

The results indicate that, by an increment in the solution pH from 4 to 10, the adsorption equilibrium capacity and the removal efficiency of 2,4-D decrease for all the adsorbents. The surface charge of 2,4-D is always negative in the pH range ($pH > Pk_a$); however, the surface charge of adsorbents depends on the relation between pH_{PZC} and solution pH. The surface charge of adsorbents is positive when $pH < pH_{PZC}$, and this is negative when $pH > pH_{PZC}$. As a result, an increase in the pH value can lead to an increase in the electrostatic interaction between the adsorbents' surface and 2,4-D molecules. In addition, the dissociation degree of 2,4-D is increased by the enhancement solution pH, and then the anion species of 2,4-D are predominant in the aqueous solution. The adsorption equilibrium capacities of AC, Fe^0/AC, TiO_2/AC, and Fe^0/TiO_2/AC adsorbents decrease from 70.7 to 67.8, 73.6 to 69.5, 73.4 to 68.4, and 75.8 to 71.5 mg of adsorbate/g of the adsorbent, respectively, due to an increase in the solution pH from 4 to 10 at the initial concentration of 90 mg/L. In a similar condition, the removal efficiency of 2,4-D decreases from 78.5% to 75.3%, 81.8% to 77.2%, 81.5% to 75.9%, and 84.1% to 79.4%, respectively.

3.3. Effect of pollutant initial concentration and contact time on the 2,4-D adsorption

Figure 6 demonstrates the effect of the 2,4-D initial concentration at 15, 30, 45, 60, 75, and 90 mg/L with solution pH of 4 at 25°C. The adsorption equilibrium capacities of AC, Fe^0/AC, TiO_2/AC, and Fe^0/TiO_2/AC adsorbents increase from 14.3 to 70.7, 14.4 to 73.6, 14.3 to 73.4, and 14.5 to 75.8 mg of adsorbate/g of the adsorbent by increasing the 2,4-D initial concentration within 15-90 mg/L, respectively, because the driving force (concentration gradient) is enhanced at the higher initial concentrations. In addition, the collision between 2,4-D molecules and surface adsorbent is increased. The removal efficiencies of 2,4-D for AC, Fe^0/AC,TiO_2/AC, and Fe^0/TiO_2/AC adsorbents are decreased from 95.3% to 78.5%, 96% to 81.8%, 95.5% to 81.5%, and 96.8% to 84.2%, respectively, while the initial concentration changes from 15 to 90 mg/L at pH = 4. Furthermore, since the adsorption process is faster at the smaller concentration of adsorbate, the rate of adsorption is decreased by increasing 2,4-D initial concentration.

Figure 6 indicates the influence of contact time on the removal efficiency at different 2,4-D initial concentrations and pH = 4. The adsorption rate increased quickly with contact time at the initial times and, then, decreased gradually until equilibrium was achieved after 6-8 hours for all the initial concentrations and adsorbents at pH = 4. The observed faster rate at the initial times could be due to the presence and availability of unoccupied active sites on the surface of adsorbents. However, the active sites are occupied gradually, and the adsorption rate is decreased.

3.4. Effect of adsorbent type on the 2,4-D adsorption

The presence of the functional groups, solubility in water, polarity, ionic nature, bonding mechanism properties are the impressible parameters of the adsorption efficiency depending on the surface chemistry and adsorbate chemical properties [68]. The removal efficiencies of AC, Fe^0/AC, TiO_2/AC, and Fe^0/TiO_2/AC

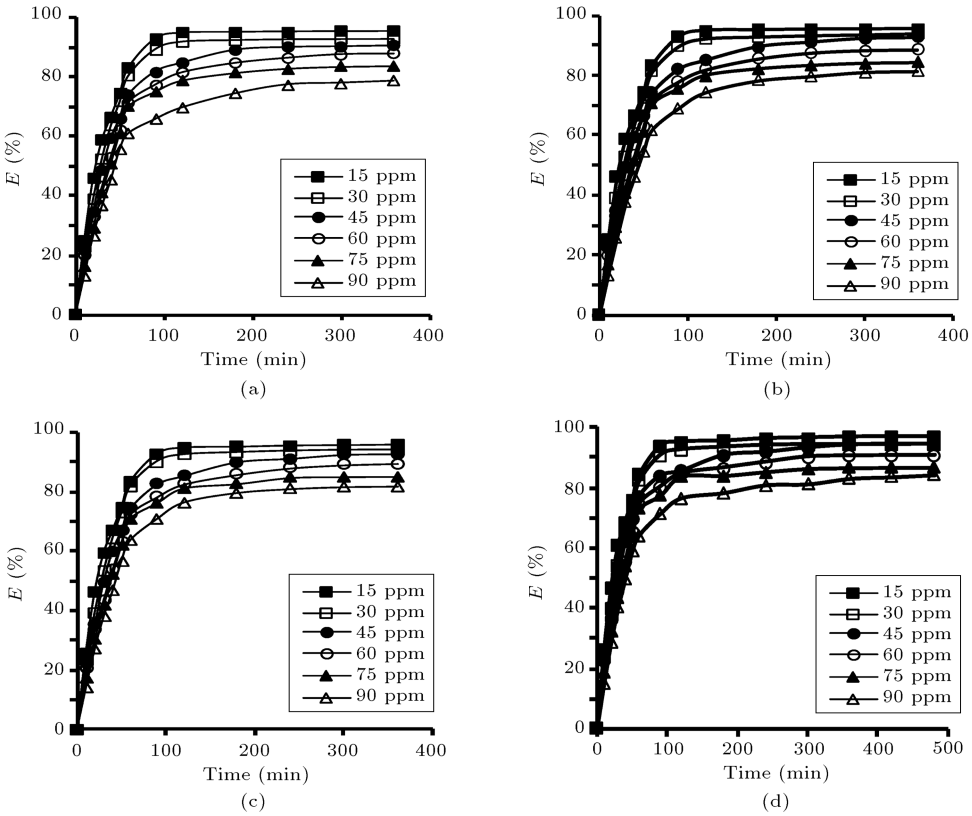

Figure 6. Effect of initial concentration and contact time of 2,4-D on the removal efficiency: (a) AC, (b) Fe^0/AC, (c) TiO_2/AC, and (d) Fe^0/TiO_2/AC (pH = 4, adsorbent = 1 g/L, $T = 25°C$, agitation speed = 130 rpm).

adsorbents are 78.5%, 81.8%, 81.5%, and 84.2%, respectively, at the initial concentration of 2,4-D 90 mg/L and pH = 4. Although the specific surface areas of the synthesized adsorbents are less than that of the AC, the removal efficiency of 2,4-D by the synthesized adsorbents is higher than that by the AC. It is explained that a combined contaminant removal by a reduction reaction on the surface of ZVI reductant and physical adsorption co-precipitation processes may occur. The contaminant is adsorbed either on ZVI and AC surfaces or is co-precipitated on the formed iron oxide/oxyhydroxide surface in ZVI/H_2O system [69]. The contaminant may be also degraded by the reactive oxygen species, produced through reaction of ZVI with the dissolved oxygen molecules [70]. The interaction between TiO_2 and oxygen molecules or water molecules may also lead to the production of oxidative agents; hence, the 2,4-D concentration in solution is reduced [71].

3.5. Adsorption kinetics

The kinetic data fit the nonlinear form of pseudo-first-order and pseudo-second-order kinetic models using the curve fitting toolbox of Matlab software 2013, as shown in Figure 7.

The Lagergren pseudo-first-order model [72] is expressed by Eq. (4):

$$q_t = q_e \left(1 - e^{-k_1 t}\right), \tag{4}$$

where k_1 (1/min), q_e (mg/g), and t (min) are the pseudo-first-order kinetic rate constant, adsorption equilibrium capacity, and contact time, respectively.

The pseudo-second-order model [73] is represented by Eq. (5):

$$q_t = \frac{k_2 q_e^2 t}{(1 + k_2 q_e t)}, \tag{5}$$

where k_2 (g/mg min) is the pseudo-second-order rate constant.

The correlation coefficient (R^2) and Root-Mean-Square Error (RMSE) are computed to evaluate the fitting goodness. The RMSE is used to determine the most appropriately practical model. The obtained kinetic parameters for the pseudo-first-order and pseudo-second-order kinetic models are summarized in Table 3.

The adsorption of 2,4-D onto all adsorbents is best explained by the pseudo-first-order kinetic model. The result demonstrates that the adsorption is more inclined towards physisorption.

The Weber-Morris model (intraparticle diffusion) [74] is applied to define the adsorption mechanism. It is expressed by Eq. (6):

$$q_t = k_i t^{0.5} + C_i, \tag{6}$$

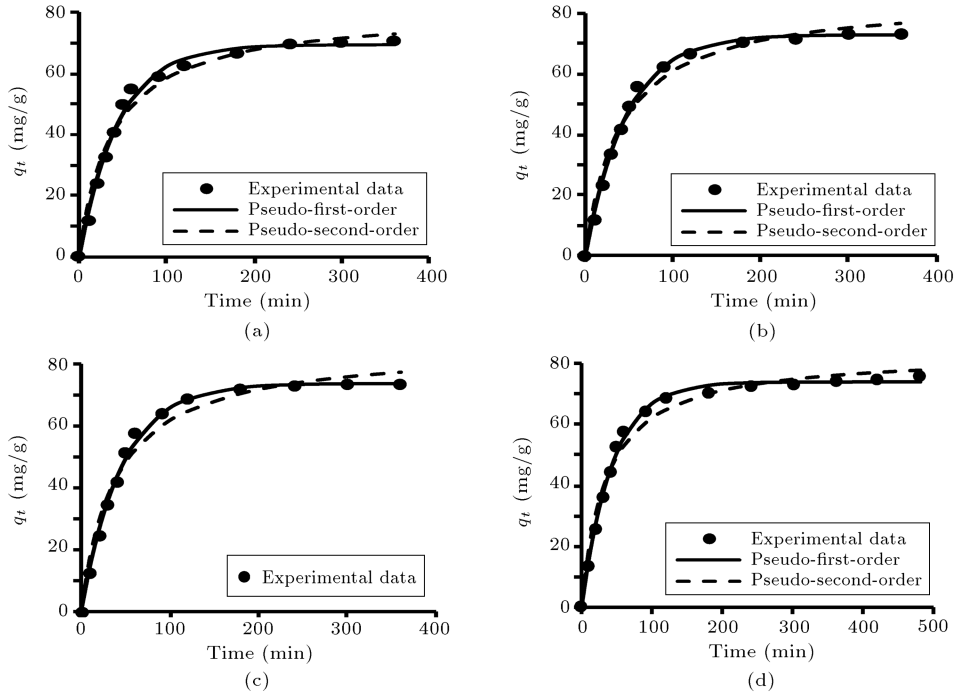

Figure 7. Plots of kinetic models for the adsorption of 2,4-D onto: (a) AC, (b) Fe^0/AC, (c) TiO_2/AC, and (d) Fe^0/TiO_2/AC (pH = 4, C_0 = 90 mg/L, adsorbent = 1 g/L, T = 25°C, agitation speed = 130 rpm).

Table 3. Kinetic parameters for the adsorption of 2,4-D.

Model	Parameter	Adsorbent			
		AC	**Fe^0/AC**	**TiO_2/AC**	**Fe^0/TiO_2/AC**
	q_e^{exp} (mg/g)	70.66	73.64	73.39	75.77
Pseudo-first-order	k_1 (1/min)	0.0225	0.0221	0.0215	0.0232
	q_e (mg/g)	69.53	73.77	72.96	73.98
	R^2	0.9941	0.9965	0.9970	0.9966
	RMSE	1.8855	1.5466	1.421	1.4915
Pseudo-second-order	k_2 (g/mg min)	0.00032	0.000298	0.00029	0.00035
	q_e (mg/g)	81.02	85.99	85.41	83.29
	R^2	0.9837	0.9801	0.9835	0.9835
	RMSE	3.1458	3.6957	3.3402	3.2712

where k_i (mg/g $min^{0.5}$) and C_i are the intraparticle diffusion rate constant and the thickness of boundary layer, respectively.

There are three forms for the regression of $q_t = f(t^{0.5})$. The intraparticle diffusion is the dominant mechanism of the adsorption procedure, when the regression is linear and intercept is equal to zero ($C_i = 0$). The intraparticle diffusion participates in adsorption mechanism, but not as the limiting step, when the regression is linear and intercept is not equal to zero ($C_i \neq 0$). The multi-linear plot illustrates that the adsorption mechanism incorporates different steps. The initial and second sections of the diagram represent external adsorption and intraparticle diffusion, respectively [26]. In this study, the regression is linear and intercept is not equal to zero ($C_i \neq 0$); therefore, the intraparticle diffusion participates in adsorption mechanism, but not as the limiting step (Figure 8).

3.6. Adsorptions isotherms

The adsorption equilibrium data are in agreement with the nonlinear form of Langmuir, Freundlich, Tempkin, and Redlich-Peterson isotherm models.

The Langmuir isotherm [75] is reliable for monolayer adsorption; it is in accordance with the monolayer envelopment and homogeneous adsorbent surface assumption, represented by Eq. (7):

$$q_e = \frac{q_m K_L C_e}{1 + K_L C_e}, \tag{7}$$

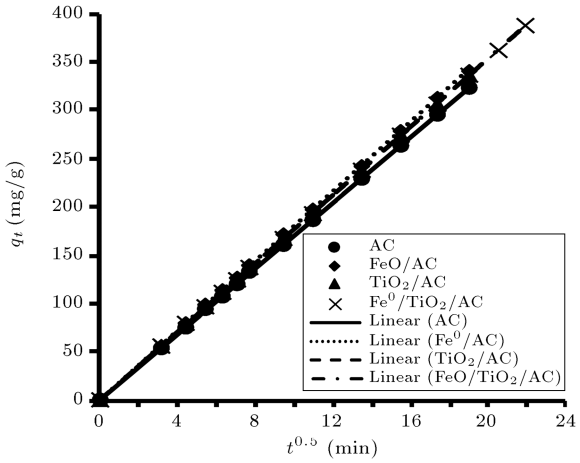

Figure 8. Plots of Weber-Morris model for adsorption mechanism of the 2,4-D (pH = 4, C_0 = 90 mg/L, adsorbent = 1 g/L, T = 25°C, and agitation speed = 130 rpm).

where q_m (mg/g) is the monolayer adsorption capacity, and K_L (L/mg) is an isotherm constant related to the free energy of adsorption.

The Langmuir isotherm can be defined using a dimensionless constant separation factor R_L [76] that is given by Eq. (8):

$$R_L = \frac{1}{1 + bC_0}, \tag{8}$$

where C_0 (mg/L) is the highest initial concentration of adsorbate, and b (L/mg) is Langmuir constant.

The value of R_L shows the adsorption process which may be undesirable ($R_L > 1$), linear ($R_L = 1$), desirable ($0 < R_L < 1$) or irreversible ($R_L = 0$).

The Freundlich isotherm [77] is an experimental model. It is in accordance with the hypothesis of multi-layer adsorbate structure formation onto an adsorbent's heterogeneous surface. In addition, it is considered that the binding strength reduces through the enhancement of the site occupation and is expressed by Eq. (9):

$$q_e = K_F (C_e)^{\frac{1}{n}}, \tag{9}$$

where K_F (mg/g(mg/L)^n) and n are Freundlich isotherms related to the adsorption capacity and adsorption intensity, respectively.

The Tempkin isotherm [78] is in accordance with the supposition that the adsorption heat declines linearly with surface envelopment, because there is an interaction between adsorbate and adsorbate. It is explained by Eq. (10):

$$q_e = B ln (K_T C_e), \tag{10}$$

where $B = RT/b$, b (J/mol) is the isotherm constant and related to the heat of adsorption; R (8.314 J/mol.k) is the universal gas constant; T (K) is the absolute temperature; K_T (L/g) is the Tempkin isotherm constant which is related to the most binding energy.

The numerator and denominator of Redlich-Peterson isotherm equation have a linear and an exponential relationship with the adsorbate concentration, respectively. It is given by Eq. (11):

$$q_e = \frac{K_{RP} C_e}{1 + a_{RP} C_e^{\beta}}, \tag{11}$$

where K_{RP} (L/g), a_{RP} (L/mg)$^{\beta}$, and β are the isotherm parameters. K_{RP} is related to the adsorption capacity, and β is related to the adsorption nature. For $\beta = 1$, Eq. (11) converts to the Langmuir equation [79].

The 2,4-D adsorption equilibrium data fit the isotherm models by nonlinear regression over the experimental data, and the main results are presented in Figure 9 and Table 4.

The comparison of R^2 and RMSE values among the four models indicates that the Redlich-Peterson is an appropriate isotherm to fit the 2,4-D experimental adsorption data onto the AC, Fe^0/AC, TiO_2/AC and Fe^0/TiO_2/AC adsorbents. The amount of β that is close to 1 represents the Langmuir isotherm which is also suitable; moreover, R^2 and RMSE values of the Langmuir and Redlich-Peterson isotherms are close together according to the data in Table 4. Therefore, the Langmuir isotherm fits the experimental data, showing a homogeneous distribution of active sites on the surface of adsorbents and the monolayer adsorption mechanism. In addition, R_L value is determined to be within 0 and 1 for all the adsorbents and at all pHs, illustrating a desirable adsorption. The monolayer adsorption capacities for AC, Fe^0/AC, TiO_2/AC, and Fe^0/TiO_2/AC are 86.5, 87.5, 86.57, and 88.76 mg of adsorbate/g of adsorbent, respectively, at pH = 4.

Table 5 illustrates an evaluation of the monolayer adsorption capacity of 2,4-D with different types of activated carbon adsorbents [1,80], and the results of this study are compared with the previous studies. According to the obtained monolayer adsorption capacity, it can be concluded that the adsorbents' capacity of this study can be comparable to the adsorbents' capacity of the previous studies.

4. Conclusion

Fe^0/AC, TiO_2/AC, and Fe^0/TiO_2/AC adsorbents adsorbed 2,4-D without any adsorption capacity reduction as compared to AC. The adsorption equilibrium data better fitted the Langmuir isotherm. The kinetic results indicated that the pseudo-first-order kinetic model managed to describe the adsorption process perfectly. By an increase in the solution pH from

Table 4. Isotherm parameters for the adsorption of 2,4-D at 25°C and pH = 4, 7, 10.

pH value	Isotherm model	Parameter	Adsorbent			
			AC	**Fe^0/AC**	**TiO_2/AC**	**Fe^0/TiO_2/AC**
4	Langmuir	K_L (L/mg)	0.2178	0.2738	0.263	0.3188
		q_m (mg/g)	86.5	87.5	86.57	88.76
		R_L	0.049-0.23	0.039-0.196	0.04-0.202	0.034-0.173
		R^2	0.9955	0.9942	0.9907	0.9832
		RMSE	1.6076	1.8986	2.3829	3.3203
	Freundlich	K_F (mg/g)(mg/L)^n	21.04	23.37	22.42	25.2
		n	2.356	2.377	2.338	2.379
		R^2	0.9796	0.9793	0.9799	0.9769
		RMSE	3.4189	3.5781	3.4961	3.9013
	Tempkin	K_T (L/g)	2.711	3.205	2.909	3.903
		B	17.55	18.08	18.25	18.07
		R^2	0.9871	0.9911	0.9922	0.9798
		RMSE	2.7182	2.3541	2.1741	3.6491
	Redlich-Peterson	K_{RP} (L/g)	25.16	32.43	32.25	44.85
		aR_P (L/mg)$^\beta$	0.4662	0.5877	0.6333	0.9126
		β	0.8532	0.8471	0.8249	0.7956
		R^2	0.9983	0.9977	0.9955	0.9896
		RMSE	1.1250	1.3678	1.9037	3.0152
7	Langmuir	K_L [L/mg]	0.1911	0.2281	0.2126	0.2738
		q_m (mg/g)	86.16	86.78	86.47	88.15
		R_L	0.055-0.259	0.038-0.19	0.045-0.22	0.029-0.153
		R^2	0.9981	0.9953	0.9966	0.9899
		RMSE	1.0094	1.6640	1.3883	2.5186
	Freundlich	K_F (mg/g)(mg/L)^n	19.54	21.35	20.54	23.4
		n	2.311	2.341	2.322	2.352
		R^2	0.9727	0.9814	0.9796	0.9815
		RMSE	3.8704	3.2948	3.4059	3.4033
	Tempkin	K_T (L/g)	2.158	2.752	2.483	3.35
		B	18.06	17.78	17.92	17.97
		R^2	0.9912	0.9890	0.9908	0.9850
		RMSE	2.1917	2.5346	2.2824	3.0724
	Redlich-Peterson	K_{RP} (L/g)	18.4	27.02	23.53	36.59
		a_{RP} (L/mg)$^\beta$	0.268	0.5131	0.4191	0.7433
		β	0.9306	0.842	0.8653	0.8066
		R^2	0.9987	0.9986	0.999	0.9952
		RMSE	0.9712	1.0379	0.8901	2.0021

Table 4. Isotherm parameters for the adsorption of 2,4-D at 25°C and pH = 4, 7, 10 (continued).

pH value	Isotherm model	Parameter	Adsorbent			
			AC	Fe^0/AC	TiO_2/AC	$Fe^0/TiO_2/AC$
10	Langmuir	K_L (L/mg)	0.1614	0.186	0.1692	0.2205
		q_m (mg/g)	85.71	86.27	86.19	87.47
		R_L	0.064-0.29	0.056-0.264	0.062-0.283	0.048-0.23
		R^2	0.9966	0.9921	0.995	0.9920
		RMSE	1.3232	2.0777	1.633	2.1618
	Freundlich	K_F (mg/g)(mg/L)^n	17.49	19.18	18.13	21.24
		n	2.224	2.285	2.246	2.336
		R^2	0.9729	0.9762	0.9728	0.9769
		RMSE	3.7478	3.6050	3.7937	3.6716
	Tempkin	K_T (L/g)	1.721	2.237	1.888	2.758
		B	18.35	17.7	18.15	17.7
		R^2	0.9909	0.9815	0.9866	0.9810
		RMSE	2.1719	3.1784	2.6647	3.3295
	Redlich-Peterson	K_{RP} (L/g)	14.93	20.16	16.16	25.31
		a_{RP} (L/mg)$^\beta$	0.2085	0.3584	0.2359	0.4561
		β	0.9462	0.8701	0.931	0.857
		R^2	0.9969	0.9938	0.9954	0.9943
		RMSE	1.4627	2.1236	1.7979	2.1104

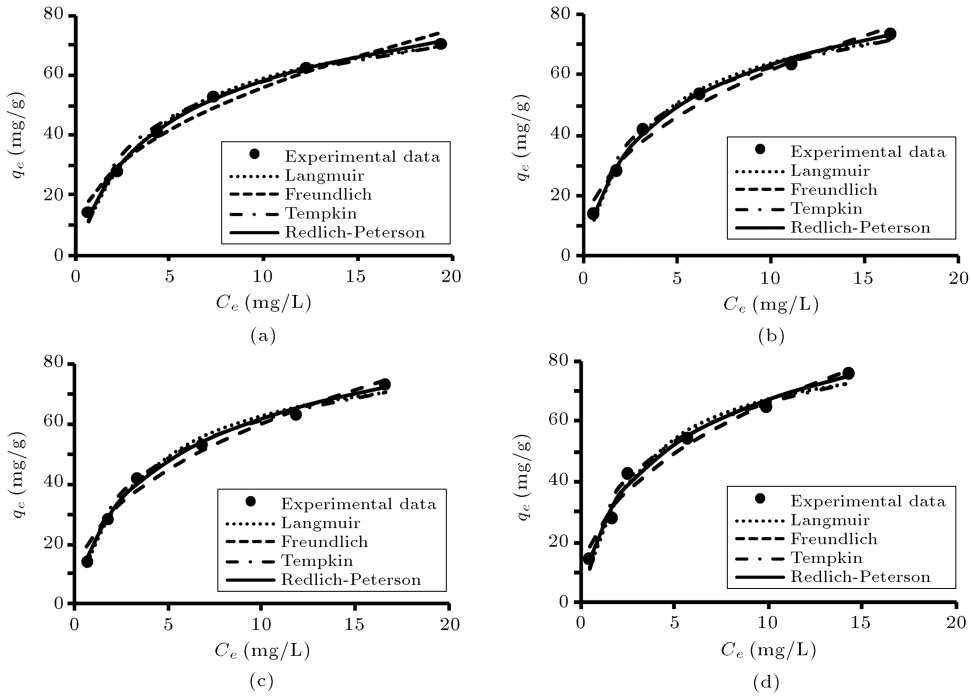

Figure 9. Plots of isotherm models for the adsorption of 2,4-D onto: (a) AC, (b) Fe^0/AC, (c) TiO_2/AC, and (d) $Fe^0/TiO_2/AC$ (pH = 4, adsorbent = 1 g/L, T = 25°C and agitation speed = 130 rpm).

Table 5. Comparison of monolayer adsorption capacity of 2,4-D onto various activated carbon.

AC type	Condition	BET Surface area (m^2/g)	q_m (mg/g)	References
AP21	50-400 mg/L, 25°C	427.8	51.02	[1]
AZ21	50-400 mg/L, 25°C	453.8	59.77	[1]
AN13	50-400 mg/L, 25°C	498.9	80	[1]
Sesame Stalk (SSAC)	100-500 mg/L, 20°C	490	49.02	[80]
Powder (PAC)	15-90 mg/L, 25°C	447.7	86.5	This study
Fe^0/AC	15-90 mg/L, 25°C	364.6	87.7	This study
TiO_2/AC	15-90 mg/L, 25°C	447.2	86.57	This study
Fe^0/TiO_2/AC	15-90 mg/L, 25°C	402.1	88.76	This study

4 to 10 and the 2,4-D initial concentration from 15 to 90 mg/L, the adsorption equilibrium capacity decreased for all the adsorbents at 25°C. In future research, the adsorption capacity of Fe^0/TiO_2/AC adsorbent along with its photocatalytic degradation characteristic in the presence of light illumination and oxidative agents will be examined for enhancing 2,4-D removal performance. In addition, further investigation is required to commercialize Fe^0/TiO_2/AC adsorbents.

Acknowledgment

The authors would like to acknowledge Iranian National Nanotechnology Initiative for the scientific assistance in the respect.

Nomenclature

$2,4-D$	2,4-dichlorophenoxyacetic acid
t	Contact time (min)
q_t	Adsorption capacity at time t (mg/g)
C_0	Initial concentration of pollutant (mg/L)
C_t	Concentration at t (mg/L)
V	Volume of the pollutant solution (L)
m	Mass of the adsorbent (g)
C_e	Equilibrium concentration of pollutant (mg/L)
k_1	Pseudo-first-order kinetic rate constant (1/min)
q_e	Equilibrium adsorbed 2,4-D on the adsorbent (mg/g)
k_2	Pseudo-first-order kinetic rate constant (g/mg min)
R^2	Correlation coefficient
RMSE	Root-Mean Square Error
k_i	Intraparticle diffusion rate constant (mg/g $min^{0.5}$)
C_i	Thickness of boundary layer
q_m	Maximum adsorption capacity (mg/g)
K_L	Langmuir isotherm constant (L/mg)
R_L	Separation factor
C_0	Highest initial concentration of adsorbate (mg/L)
n	Freundlich isotherm constant
K_F	Freundlich isotherm constant $(mg/g(mg/L)^n)$
B	Tempkin isotherm constant
b	Isotherm constant (J/mol)
R	Universal gas constant (J/mol.K)
T	Absolute temperature (K)
K_T	Tempkin isotherm constant (L/g)
K_{RP}	Redlich-Peterson isotherm constant (L/g)
a_{RP}	Redlich-Peterson isotherm constant $(L/mg)^\beta$
β	Redlich-Peterson isotherm constant
E	Efficiency (%)

References

1. Youssef, A.M., El-Didamony, H., El-Sharabasy, S.F., Sobhy, M., Hassan, A.F., and Bolaneke, R. "Adsorption of 2,4-dichlorophenoxyacetic acid on different types of activated carbons based date palm pits: kinetic and thermodynamics studies", *Int. Res. J. Pure Appl. Chem.*, **14**(1), pp. 1-15 (2017).
2. Cansado, I.P.P., Mourao, P.A.M., Gomez, J.A.F.L., and Almodovar, V. "Adsorption of MCPA, 2,4-D and diuron onto activated carbons from wood composites", *Ciência & Tecnologia dos Materiais*, **29**, pp. 224-228 (2017).
3. Trivedi, N.S., Kharkar, R.A., and Mandavgane, S.A. "2,4-dichlorophenoxyacetic acid adsorption on adsorbent prepared from groundnut shell: Effect of preparation conditions on equilibrium adsorption capacity", *Arab. J. Chem.*, **7**, pp. 22-31 (2016).

4. Bazrafshan, E., Mostafapour, F.K., Faridi, H., Farzadkia, M., Sargazi, S., and Sohrabi, A. "Removal of 2,4-dichlorophenoxyacetic acid (2,4-D) from aqueous environments using single-walled carbon nanotubes", *Health Scope*, **2**(1), pp. 39-46 (2013).
5. Lu, X., Shao, Y., Gao, N., and Ding, L. "Equilibrium, thermodynamic, and kinetic studies of the adsorption of 2,4-dichlorophenoxyacetic acid from aqueous solution by MIEX resin", *J. Chem. Eng. Data.*, **60**(5), pp. 1259-1269 (2015).
6. Li, Q., Sun, J., Ren, T., Guo, L., Yang, Z., Yang, Q., and Chen, H. "Adsorption mechanism of 2,4-dichlorophenoxyacetic acid onto nitric acid modified activated carbon fiber", *Environ. Technol.*, **39**(7), pp. 895-906 (2018).
7. Njoku, V.O., Islam, M.A., Asif, M., and Hameed, B. "Adsorption of 2,4-dichlorophenoxyacetic acid by mesoporous activated carbon prepared from H3PO4-activated langsat empty fruit bunch", *J. Environ. Manage.*, **154**, pp. 138-144 (2015).
8. Schenone, A.V., Conte, L.O., Botta, M.A., and Alfano, O.M. "Modeling and optimization of photo-Fenton degradation of 2,4-D using ferrioxalate complex and response surface methodology (RSM)", *J. Environ. Manage.*, **155**, pp. 177-183 (2015).
9. *Guidelines for Drinking-Water Quality*, 4th Ed incorporating the first addendum, pp. 347-348, World Health Organization, Geneva (2017).
10. Njoku, V.O., Foo, K.Y., and Hameed, B.H. "Microwave-assisted preparation of pumpkin seed hull activated carbon and its application for the adsorptive removal of 2,4-dichlorophenoxyacetic acid", *Chem. Eng. J.*, **215**, pp. 383-388 (2013).
11. Bian, X., Chen, J., and Ji, R. "Degradation of 2,4-dichlorophenoxyacetic acid (2,4-D) by novel photocatalytic material of tourmaline-coated TiO_2 nanoparticles: kinetic study and model", *Materials*, **6**(4), pp. 1530-1542 (2013).
12. Sahinkaya, S., Özdemir, C., and Onüçyildiz, M. "Treatment of pesticide wastewater by physicochemical and fenton processes", *Asian J. Chem.*, **20**(5), pp. 3795-3804 (2008).
13. Sahithya, K. and Das, N. "Remediation of pesticides using nanomaterials: an overview", *Int. J. Chem. Tech. Res.*, **8**(8), pp. 86-91 (2015).
14. Rojas, R., Morillo, J., Usero, J., Vanderlinden, E., and El Bakouri, H. "Adsorption study of low-cost and locally available organic substances and a soil to remove pesticides from aqueous solutions", *J. Hydrol*, **520**, pp. 461-472 (2014).
15. Deokar, S.K. and Mandavgane, S.A. "Estimation of packed-bed parameters and prediction of breakthrough curves for adsorptive removal of 2,4-dichlorophenoxyacetic acid using rice husk ash", *J. Environ. Chem. Eng.*, **3**(3), pp. 1827-1836 (2015).
16. Shirmardi, M., Alavi, N., Lima, E.C., Takdastan, A., Mahvi, A.H., and Babaei, A.A. "Removal of atrazine as an organic micro-pollutant from aqueous solutions: A comparative study", *Process Saf. Environ.*, **103**, pp. 23-35 (2016).
17. Taha, S.M., Amer, M.E., Elmarsafy, A.E., and Elkady, M.Y. "Adsorption of 15 different pesticides on untreated and phosphoric acid treated biochar and charcoal from water", *J. Environ. Chem. Eng.*, **2**(4), pp. 2013-2025 (2014).
18. Vukčević, M.M., Kalijadis, A.M., Vasiljević, T.M., Babić, B.M., Laušević, Z.V., and Laušević, M.D. "Production of activated carbon derived from waste hemp (Cannabis sativa) fibers and its performance in pesticide adsorption", *Micropor. Mesopor. Mat.*, **214,** pp. 156-165 (2015).
19. De Smedt, C., Ferrer, F., Leus, K., and Spanoghe, P. "Removal of pesticides from aqueous solutions by adsorption on zeolites as solid adsorbents", *Adsorpt. Sci. Technol.*, **33**(5), pp. 457-485 (2015).
20. Huong, P.T., Lee, B.K., and Kim, J. "Improved removal of 2-chlorophenol by a synthesized Cu-nano zeolite", *Process Saf. Environ.*, **100**, pp. 272-280 (2016).
21. Davies, J.E.D. and Jabeen, N. "The adsorption of herbicides and pesticides on clay minerals and soils. Part 2. Atrazine", *J. Incl Phenom. Macro. Chem.*, **46**(1), pp. 57-64 (2003).
22. Clausen, L., Fabricius, I., and Madsen, L. "Adsorption of pesticides onto quartz, calcite, kaolinite, and α-alumina", *J. Environ. Qual*, **30**(3), pp. 846-857 (2001).
23. Abdeen, Z. and Mohammad, S.G. "Study of the adsorption efficiency of an eco-friendly carbohydrate polymer for contaminated aqueous solution by organophosphorus pesticide", *Open Journal of Organic Polymer Materials*, **4**(1), pp. 16-28 (2013).
24. Carneiro, R.T.A., Taketa, T.B., Neto, R.J.G., Oliveira, J.L., Campos, E.V.R., de Moraes, M.A., da Silva, C.M.G., Beppu, M.M., and Fraceto, L.F. "Removal of glyphosate herbicide from biopolymer membranes", *J. Environ. Manage.*, **151**, pp. 353-360 (2015).
25. Xu, C.-H., Zhu, L.-J., Wang, X.-H., Lin, S., and Chen, Y.-M. "Fast and highly efficient removal of chromate from aqueous solution using nanoscale zero-valent iron/activated carbon (NZVI/AC)", *Water Air Soil. Pollut.*, **225**(2), pp. 1845-1857 (2014).
26. Aksu, Z. and Kabasakal, E. "Batch adsorption of 2,4-dichlorophenoxyacetic acid (2,4-D) from aqueous solution by granular activated carbon", *Sep. Purif. Technol.*, **35**(3), pp. 223-240 (2004).
27. Dehghani, M., Nasseri, S., and Karamimanesh, M. "Removal of 2,4-dichlorophenolyxacetic acid (2,4-D) herbicide in the aqueous phase using modified granular activated carbon", *Iranian J. Environ. Health Sci. Eng.*, **12**(1), pp. 28-38 (2014).
28. Hameed, B.H., Salman, J.M., and Ahmad, A.L. "Adsorption isotherm and kinetic model of 2,4-D pesticide on activated carbon derived from date stones", *J. Hazard. Mater.*, **163**, pp. 121-126 (2009).

29. Jassem, M.S., Abdulkarim, M., and Huda S.H. "Adsorption of 2,4-dichlorophenoxyacetic acid onto coconut activated carbon: kinetics and equilibrium studies", *Al-Mustansiriyah J. Sci.*, **22**(6), pp. 377-384 (2009).

30. Njoku, V.O. and Hameed B.H. "Preparation and characterization of activated carbon from corncorb by chemical activation by H_3PO_4 for 2,4-dichlorophenoxyacetic acid adsorption", *Chem. Eng. J.*, **173**, pp. 391-399 (2011).

31. Njoku, V.O., Asif, M., and Hameed, B.H. "2,4-dichlorophenoxyacetic acid adsorption onto coconut shell-activated carbon: isotherm and kinetic modeling", *Desalin. Water Treat.*, **55**(1), pp. 132-141 (2015).

32. Salman, J.M. and Al-Saad, K.A. "Adsorption of 2,4-dichlorophenoxyacetic acid onto data seeds activated carbon: equilibrium, kinetic and thermodynamic studies", *Int. J. Chem. Sci.*, **10**(2), pp.677-690 (2012).

33. Salman, J.M. and Hameed B.H. "Adsorption of 2,4-dichlorophenoxyacetic acid and carbofuran pesticides onto granular activated carbon", *Desalination*, **256**, pp. 129-135 (2010).

34. Khoshnood, M. and Azizian, S. "Adsorption of 2,4-dichlorophenoxyacetic acid pesticide by graphitic carbon nanostructures prepared from biomasses", *J. Ind. Eng. Chemi.*, **18**(5), pp. 1796-1800 (2012).

35. Cheng, Y., Jing, L., and Zongshan, Z. "Effective organochlorine pesticides removal from aqueous systems by magnetic nanospheres coated with polystyrene", *J. Wuhan Univ. Technol-Mater. Sci. Ed.*, **29**(1), pp. 168-173 (2014).

36. Fu, F., Ma, J., Xie, L., Tang, B., Han, W., and Lin, S. "Chromium removal using resin supported nanoscale zero-valent iron", *J. Environ. Manage.*, **128**, pp. 822-827 (2013).

37. Shi, J., Long, C., and Li, A. "Selective reduction of nitrate into nitrogen using Fe-Pd bimetallic nanoparticle supported on chelating resin at near-neutral pH", *Chem. Eng. J.*, **286**, pp. 408-412 (2016).

38. Chekli, L., Bayatsarmadi, B., Sekine, R., Sarkar, B., Shen, A.M., Scheckel, K.G., Skinner, W., Naidu, R., Shon, H.K., Lombi, E., and Donner, E. "Analytical Characterization of nanoscale zero-valent iron: An illustrated methodological review", *Anal. Chim. Acta.*, **903**, pp. 13-35 (2016).

39. Kakavandi, B., Kalantary, R.R., Farzadkia, M., Mahvi, A.H., Esrafili, A., Azari, A., Yari, A.R., and Javid, A.B. "Enhanced chromium (VI) removal using activated carbon modified by zero valent iron and silver bimetallic nanoparticles", *Iranian J. Environ. Health Sci. Eng.*, **12**(1), pp. 115-125 (2014).

40. Ling, X., Li, J., Zhu, W., Zhu, Y., Su, X., Shen, J., Han, W., and Wang, L. "Synthesis of nanoscale zero-valent iron/ordered mesoporous carbon for adsorption and synergistic reduction of nitrobenzene", *Chemosphere*, **87**(6), pp. 655-660 (2012).

41. Quan, G., Sun, W., Yan, J., and Lan, Y. "Nanoscale zero-valent iron supported on biochar: characterization and reactivity for degradation of acid orange 7 from aqueous solution", *Water Air Soil. Pollut.*, **225**(11), pp. 2195-2205 (2014).

42. Wang, C., Luo, H., Zhang, Z., Wu, Y., Zhang, J., and Chen, S. "Removal of As(III) and As(V) from aqueous solution using nanoscale zero valent iron-reduced graphite oxide modified composites", *J. Hazard. Mater.*, **268**, pp. 124-131 (2014).

43. Lu, H., Qiao, X., Wang, W., Tan, F., Xia, Z., and Chen, J. "Facile preparation of mesoporous silica/nano zero-valent iron composite for Pb (II) removal from aqueous solution", *Desalin. Water Treat.*, **57**(23), pp. 10745-10756 (2016).

44. Hameed, A.K., Rahim, M.H.A., Dewayanto, N., and Nordi, M.R. "Adsorption study of chloroform onto zero valent iron supported on mesoporous silica", *Adv. Appl. Sci. Res.*, **8**(2), pp. 62-68 (2017).

45. Chi, Z., Wang, Z., Chu, H., Bin, P., and Lucian, L. "Bentonite-supported nanoscale zero-valent iron granulated electrodes for industrial wastewater remediation", *RSC Adv.*, **7**, pp. 44605-44613 (2017).

46. Georgiou, Y., Dimos, K., Beltsios, K., Karakassides, M.A., and Deligiannakis, Y. "Hybrid [Polysulfone-zero valent iron] membranes: synthesis, characterization and application for AsIII remediation", *Chem. Eng. J.*, **281,** pp. 651-660 (2015).

47. Padil, V.V.T., Filip, J., Suresh, K.I., Wacławek, S., and Černík, M. "Electrospun membrane composed of poly[Acrylonitrile-co-(Methyl acrylate)-co-(Itaconic acid)] terpolymer and ZVI nanoparticles and its application for the removal of arsenic from water", *RSC Adv.*, **6**, pp. 110288-110300 (2016).

48. Mohammadi, A. and Karimi, A.A. "Methylene blue removal using surface-modified TiO_2 nanoparticles: A comparative study on adsorption and photocatalytic degradation", *J. Water Environ. Nanotechnol.*, **2**(2), pp. 118-128 (2017).

49. Selishchev, D., Kolinko, P., and Kozlov, D. "Influence of adsorption on the photocatalytic properties of TiO_2/AC composite materials in the acetone and cyclohexane vapor photooxidation reactions", *J. Photochem. Photobiol. A.*, **229**(1), pp. 11-19 (2012).

50. Abdennouri, M., Elhalil, A., Farnane, M., Tounsadi, H., Mahjoubi, F.Z., Elmoubarki, R., Sadiq, M., Khamar, L., Galadi, A., Baalala, M., Bensitel, M., El hafiane, Y., Smith, A., and Barka, N. "Photocatalytic degradation of 2,4-D and 2,4-DP herbicides pn Pt/TiO_2 nanoparticles", *J. Saudi Chem. Soc.*, **19**, pp. 485-493 (2015).

51. Kudlek, E., Silvestri, D., Waclawek, S., Padil, V.V.T., Stuchlik, M., Volesky, L., Kejzlar, P., and Cernik, M. "TiO_2 immobilized on biopolymer nanofibers for the removal of bisphenol A and diclofenac from water", *Ecol. Chem. Eng. S.*, **24**(3), pp. 417-429 (2017).

52. Nie, L., Wang, J., and Yu, J. "Preparation of a Pt/ TiO_2/cotton fiber composite catalyst with low air resistance for efficient formaldehyde oxidation at room temperature", *RSC Adv.*, **7**, pp. 21389-21397 (2017).

53. Pei, J., Ma, W., Li, R., Li, Y., and Du, H. "Preparation and photocatalytic properties TiO_2-Al_2O_3 composite loaded catalyst", *J. Chem.*, **2015**, pp. 1-7 (2015).

54. Zeng, Y., Xue, Y., Liang, S., and Zhang, J. "Removal of fluoride from aqueous solution by TiO_2 and TiO_2-SiO_2 nanocomposite", *Chem. Spec. Bioavailab.*, **29**(1), pp. 25-32 (2017).

55. Xing, B., Shi, C., Zhang, C., Yi, G., Chen, L., Guo, H., Huang, G., and Cao, J. "Preparation of TiO_2/activated carbon composites for photocatalytic degradation of RhB under UV light irradiation", *J. Nanomater.*, **2016**, pp. 1-10 (2016).

56. Alalm, M.G., Tawfik, A., and Ookawara, S. "Enhancement of photocatalytic activity of TiO_2 by immobilization on activated carbon for degradation of pharmaceuticals", *J. Environ. Chem. Eng.*, **4**(2), pp. 1929-1937 (2016).

57. Rosa, S.M.C., Nossol, A.B.S., Nossol, E., Zarbin, A.J.G., and Peralte-Zamora, P.G. "Non-synergistic UV-A photocatalytic degradation of estrogens by nano-TiO_2 supported on activated carbon", *J. Braz. Chem. Soc.*, **28**(4), pp. 582-588 (2017).

58. Tamilselvi, S., Asaithambi, M., and Sivakumar, P. "Nano-TiO_2-loaded activated carbon fiber composite for photodegradation of a textile dye", *Desalin. Water Treat.*, **57**(33), pp. 15495-15502 (2016).

59. Zhang, J., Liu, F., Gao, J., Chen, Y., and Hao. X. "Ordered mesoporous TiO_2/activated carbon for adsorption and photocatalysis of acid red 18 solution", *Bio Resources*, **12**(4), pp. 9086-9102 (2017).

60. Saritha, B. and Chockalingam, M.P. "Photodegradation of Malachite green dye using TiO_2/activated carbon composite", *International Journal of Civil Engineering and Technology*, **8**(8), pp. 156-163 (2017).

61. Li, Y., Chen, J., Liu, J., Ma, M., Chen, W., and Li, L. "Activated carbon supported TiO_2-photocatalysis doped with Fe ions for continuous treatment of dye wastewater in a dynamic reactor", *J. Environ. Sci.*, **22**(8), pp. 1290-1296 (2010).

62. Reddy, D.H.K., Harinath, Y., Seshaiah, K., and Reddy, A. "Biosorption of Pb (II) from aqueous solutions using chemically modified Moringa oleifera tree leaves", *Chem. Eng. J.*, **162**(2), pp. 626-634 (2010).

63. Liu, A. and Zhang, W. "Fine structural features of core-shell nanoscale zero-valent iron characterized with aberration-corrected scanning transmission electron microscopy (Cs-ATEM)", *RSC. J.*, **139**, pp. 4512-4518 (2014).

64. Li, H., Chen, Y.Q., Chen, S., Wang, X.L., Guo, S., Qiu, Y.F., Liu, Y.D., Duan, X.L., and Yu, Y.J. "Wheat straw biochar-supported nanoscale zerovalent iron for removal of trichloroethylene from groundwater", *PLoS ONE*, **12**(3), e0172337 (2017).

65. Kannaiyan, D., Kochuveedu, S.T., Jang, Y.H., Jang, Y.J., Lee, J.Y., Lee, J., Kim, J., and Kim, D.H. "Enhanced photophysical properties of nanopatterned titania nanodots/ nanowires upon hybridization with silica via block co-polymer template sol-gel process", *Polymers*, **2**, pp. 490-504 (2010).

66. Njoku, V.O., Foo, K.Y., Asif, M., and Hameed, B.H. "Preparation of activated carbons from rambutan (Nephelium lappaceum) peel by microwave-induced KOH activation for acid yellow 17 dye adsorption", *Chem. Eng. J.*, **250**, pp. 198-204 (2014).

67. Diaz-Flores, P.E., Leyva-Ramos, R., Rangel-Mendez, J.R., Ortiz, M.M., Guerrero-Coronado, R.M., and Mendoza-Barron, J. "Adsorption of 2,4- dichlorophenoxyacetic acid from aqueous solution on activated carbon cloth", *J. Environ. Eng. Manage.*, **16**(4), pp. 249-257 (2006).

68. Kim, S.J., Shim, W.G., Kim, T.Y., Moon, H., Kim, S.J., and Cho, S.Y. "Adsorption equilibrium characteristics of 2, 4-Dichlorophenoxyacetic acid and 2, 4-dinitrophenol on granular activated carbons", *Korean J. Chem. Eng.*, **19**(6), pp. 967-977 (2002).

69. Noubactep, C. "An analysis of the evolution of reactive species in Fe^0/H_2O systems", *J. Hazard. Mater.*, **168**, pp. 1626-1631 (2009).

70. Tang, J., Tang, L., Feng, H., Zeng, G., Dong, H., Zhang, C., Huang, B., Deng, Y., Wang, J., and Zhou, Y. "pH dependent degradation of p-nitrophenol by sulfidated nanoscale zerovalent iron under aerobic or anoxic condition", *J. Hazard. Mater.* (2016). http://dx.doi.org/10.1016/j.jhazmat.2016.07.042.

71. Du, Z., Zhao, C., Chen, J., and Zhang, D. "DFT study of the interactions of H_2O, O_2 and H_2O + O_2 with TiO_2 (101) surface", *Comput. Mater. Sci.*, **136**, pp. 173-180 (2017).

72. Langergren, S. and Svenska, B.K. "About the theory of so-called adsorption of soluble substances" [Zur theorie de sogenanntен adsorption geloester stoffe], *Veternskapsakad Handlingar*, **24**(4), pp. 1-39 (1898).

73. Ho, Y.S. "Review of second-order models for adsorption systems", *J. Hazard. Mater.*, **136**(3), pp. 681-689 (2006).

74. Weber, W.J. and Morris, J.C. "Kinetics of adsorption on carbon from solution", *Journal of the Sanitary Engineering Division*, **89**(2), pp. 31-60 (1963).

75. Langmuir, I. "The adsorption of gases on plane surface of glass, mica and platinum", *J. Am. Chem. Soc.*, **40**(9), pp. 1361-1403 (1918).

76. Hall, K.R., Eagleton, L.C., Acrivos, A., and Vermeulen, T. "Pore-and solid-diffusion kinetics in fixed-bed adsorption under constant-pattern conditions", *Ind. Eng. Chem. Fund.*, **5**(2), pp. 212-223 (1966).

77. Freundlich, H. "Over the adsorption in solution" [Über die adsorption in lösungen], *Zeitschrift fur Physikalische Chemie*, **57**(1), pp. 385-470 (1907).

78. Tempkin, M.I. and Pyzhev, V. "Kinetics of ammonia synthesis on promoted iron catalyst", *Acta. Phys. Chim.*, **12**(1), pp. 327-356 (1940).

79. Redlich, O. and Peterson, D.L. "A useful adsorption isotherm", *J. Phys. Chem.*, **63**(6), pp. 1024-1024 (1959).

80. Kırbıyık, Ç., Pütün, A.E. and Pütün, E. "Equilibrium, kinetic, thermodynamic studies of the adsorption of Fe(III) metal ions and 2,4-dichlorophenoxyacetic acid onto biomass-based activated carbon by $ZnCl_2$ activation", *Surf, Interface*, **8**, pp. 182-192 (2017).

Biographies

Shahrokh Jokar Baloochi received the BSc degree in Chemical Engineering from Urmia University of Technology and the MSc degree in Chemical Engineering from Isfahan University. His main research interests include water and wastewater treatment and environmental engineering in the field of chemical engineering.

Ali Reza Solaimany Nazar is currently an Associate Professor in the Chemical Engineering Department at University of Isfahan, Iran. His research interests are mainly asphaltene and wax deposition in reservoir and transportation line, adsorption and advanced oxidation process in water and wastewater treatment.

Mehrdad Farhadian is currently an Assistant Professor in the Chemical Engineering Department at University of Isfahan, Iran. He is the Head of Environmental Research Institute at University of Isfahan, Isfahan, Iran. His main research interests include water and wastewater treatment and environmental engineering in the field of chemical engineering.

Amir Goshadrou is currently an Assistant Professor in the Chemical Engineering Department at University of Isfahan, Iran. He is a Member of the Process Engineering Research Center and Environmental Research Institute with specialization in bioprocess development for biofuels and bioproducts and also works on separation process modeling and simulation.